AGU PUBLICATIONS

Geophysical Research Letters

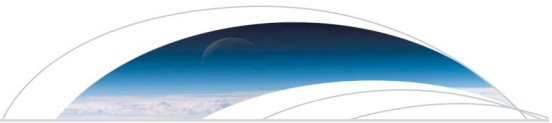

RESEARCH LETTER

10.1002/2015GL065074

Key Points:

- We present the first EM-based platelet layer thickness and conductivity data set
- Multifrequency EM data inversion enables platelet layer volume estimates
- A thicker platelet layer has a higher ice volume fraction

Supporting Information:

- Supporting Information S1

Correspondence to:
M. Hoppmann,
Mario.Hoppmann@awi.de

Citation:
Hunkeler, P. A., M. Hoppmann, S. Hendricks, T. Kalscheuer, R. Gerdes (2016), A glimpse beneath Antarctic sea ice: Platelet layer volume from multifrequency electromagnetic induction sounding, *Geophys. Res. Lett.*, *43*, doi:10.1002/2015GL065074.

Received 25 JUN 2015
Accepted 11 NOV 2015
Accepted article online 16 DEC 2015

A glimpse beneath Antarctic sea ice: Platelet layer volume from multifrequency electromagnetic induction sounding

P. A. Hunkeler[1], M. Hoppmann[1], S. Hendricks[1], T. Kalscheuer[2], and R. Gerdes[1,3]

[1]Alfred-Wegener-Institut Helmholtz-Zentrum für Polar- und Meeresforschung, Bremerhaven, Germany, [2]Department of Earth Sciences, Uppsala University, Uppsala, Sweden, [3]Earth and Space Sciences, Jacobs University Bremen, Bremen, Germany

Abstract In Antarctica, ice crystals emerge from ice shelf cavities and accumulate in unconsolidated layers beneath nearby sea ice. Such sub-ice platelet layers form a unique habitat and serve as an indicator for the state of an ice shelf. However, the lack of a suitable methodology impedes an efficient quantification of this phenomenon on scales beyond point measurements. In this study, we inverted multifrequency electromagnetic (EM) induction soundings, obtained on fast ice with an underlying platelet layer along profiles of >100 km length in the eastern Weddell Sea. EM-derived platelet layer thickness and conductivity are consistent with other field observations. Our results suggest that platelet layer volume is higher than previously thought in this region and that platelet layer ice volume fraction is proportional to its thickness. We conclude that multifrequency EM is a suitable tool to determine platelet layer volume, with the potential to obtain crucial knowledge of associated processes in otherwise inaccessible ice shelf cavities.

1. Introduction

Around Antarctica, unconsolidated accumulations of randomly oriented, individual ice crystals (platelets) are frequently observed below sea ice adjacent or attached to ice shelves. This phenomenon, hereinafter referred to as (sub-ice) platelet layer, is a consequence of basal melt processes in nearby ice shelf cavities [*Robinson et al.*, 2014; *Jordan et al.*, 2015] and part of a process referred to as "ice pump" [*Lewis and Perkin*, 1986]. This special sea ice type not only modifies the properties, mass, and energy balance of an overlying solid sea ice cover [*Eicken and Lange*, 1989; *Gough et al.*, 2012; *Hoppmann et al.*, 2015b] but also acts as a habitat for a substantial seasonal bloom of micro algae [e.g., *Günther and Dieckmann*, 1999] and provides a protective environment for coastal fish species [*Vacchi et al.*, 2000]. Ice platelets are subsequently incorporated into the solid sea ice matrix through the freezing of the interstitial water. The resulting (solid) ice type is usually referred to as incorporated platelet ice [*Langhorne et al.*, 2015] and contributes to the stabilization of breeding sites for penguins and seals. The additional buoyancy provided by the underlying platelet layer modifies the sea ice freeboard, influencing sea ice thickness retrieval by altimetry methods [*Price et al.*, 2014]. The seasonality and amount of ice platelets accumulated beneath sea ice potentially allows conclusions about processes in the ice shelf cavities [*Langhorne et al.*, 2015], which are otherwise difficult to investigate albeit their potential impact on sea ice thickness [*Hellmer*, 2004] and extent [*Bintanja et al.*, 2013] in the Southern Hemisphere.

The total volume of loose ice platelets below a sea ice cover is the product of the platelet layer thickness, area, and ice volume fraction. The platelet layer thickness is usually determined with a weighted measuring tape [*Crocker*, 1988], an approach which is time consuming and only allows for a very limited spatial coverage. The temporal evolution of platelet layer thickness is obtained by repeated drill hole measurements or by autonomous instrumentation at a fixed site [*Hoppmann et al.*, 2015a]. Ice volume fractions have been determined using a variety of methods [*Hoppmann et al.*, 2015b, and references therein] most of which are based on point measurements. *Rack et al.* [2013] used a traditional airborne EM system to measure the thickness of the McMurdo Ice Shelf and found that the presence of sub-ice platelet layers lead to an overestimation of the ice thickness. However, they were not able to resolve the thickness of the platelet layer itself. We conclude that a determination of platelet layer volume over geophysically relevant length scales still remains a challenge due to the lack of a suitable methodology.

A promising approach to efficiently determine platelet layer volume by a nondestructive method has recently been identified. *Hunkeler et al.* [2015] used the response of a ground-based, multifrequency electromagnetic (EM) induction sounding instrument to measure the electrical conductivity (hereinafter referred to as conductivity) of the platelet layer. They found an average conductivity of 1.154 S m^{-1} and calculated ice volume fractions of 0.29–0.43 using Archie's law [*Archie*, 1942] with varying cementation factors.

In the present study, we build upon these investigations and present the first consistent, high-resolution platelet layer thickness and conductivity data set recorded on Antarctic sea ice. We applied a laterally constrained Marquardt-Levenberg inversion to a unique multifrequency EM induction sounding data set obtained on immobile sea ice (fast ice) attached to an ice shelf in the eastern Weddell Sea. We tested the performance of the inversion using synthetic EM data and validated the final inversion results with drill hole measurements.

2. Methods

2.1. Field Conditions and Measurements

The area under investigation was the seasonal fast ice of Atka Bay, a sheltered embayment in the front of the Ekström Ice Shelf in the eastern Weddell Sea, Antarctica (Figures 1a and 1b). The fast ice at Atka Bay exhibits a several meter thick platelet layer and a large fraction of incorporated platelet ice, both of which have been the subject of several studies [*Kipfstuhl*, 1991; *Günther and Dieckmann*, 1999; *Hunkeler et al.*, 2015; *Hoppmann et al.*, 2015b, 2015a]. This region is also one of the rare locations around coastal Antarctica where year-round studies of sea ice are possible, due to the presence of the German wintering station Neumayer III. Sea ice at Atka Bay is characterized by a distinct seasonal cycle: a continuous sea ice cover typically establishes between March and May, destabilizing and breaking up between December and February. Between breakup and new formation, the entire bay is usually free of sea ice. The sea ice conditions in 2012, the year the present study was performed, were slightly different: during August, approximately one third of the 440 km^2 fast ice area broke up during a storm. A continuous sea ice cover was reestablished in the breakup area after a large iceberg grounded in front of Atka Bay in October. Otherwise, the sea ice conditions were comparable to other years: sea ice in the western part was deformed due to moderate ridging and rafting caused by predominantly easterly winds, while the eastern part exhibited mainly thermodynamically grown sea ice. As a result, sea ice in the east was generally thinner than the deformed sea ice of the western part. The thickest and oldest sea ice was observed in the southwestern part of Atka Bay. Drill hole measurements at several sites between June 2012 and February 2013 indicated that the platelet layer reached its spatial average maximum of around 4 m in December. Additional information is available in *Hoppmann et al.* [2015b].

We operated a commercially available multifrequency EM induction instrument (GEM-2, Geophex Ltd.) on the fast ice on four occasions between 26 November and 21 December 2012. We configured the instrument to simultaneously record GPS position and EM soundings at frequencies of 1530, 5310, 18,330, 63,030, and 93,090 Hz with a sampling rate of 10 Hz. The instrument was mounted in a kayak and pulled over the sea ice a few meters behind a snowmobile. In total, we acquired 118 km of multifrequency EM data across Atka Bay over a period of 25 days (Figure 1a and Table S1 in the supporting information). Transect 1 recorded on 26 November was excluded from all further calculations, since the frequency setup was different (no 1530 Hz data), and the same track was repeated later in December. Based on our knowledge from other studies [*Hoppmann et al.*, 2015b], we assume no significant change in platelet layer physical properties between 16 and 21 December (Table S1) and consequently regard them as one synoptic measurement.

Sea ice thickness, snow depth, and freeboard were measured with regular thickness tapes. Platelet layer thickness was determined using the metal bar method [*Crocker*, 1988], with a potential underestimation of up to 0.3 m as apparent from simultaneous real-time video. The data were already presented in *Hoppmann et al.* [2015b] and are used here for validation. Incorporated platelet ice was considered part of the solid sea ice layer in this study.

2.2. Geophysical Inversion of EM Data

A geophysical inversion algorithm calculates and iteratively adjusts a model of the subsurface, until the modeled signal response fits the measured response within its uncertainty. Sea ice with an underlying platelet layer, such as found in Atka Bay, represents a simple, almost 1-D target for geophysical inversions. In our study, we defined three separate layers: (1) sea ice plus snow, (2) the sub-ice platelet layer, and (3) seawater [*Hunkeler et al.*, 2015]. These layers are mainly characterized by their different conductivities, with distinct conductivity

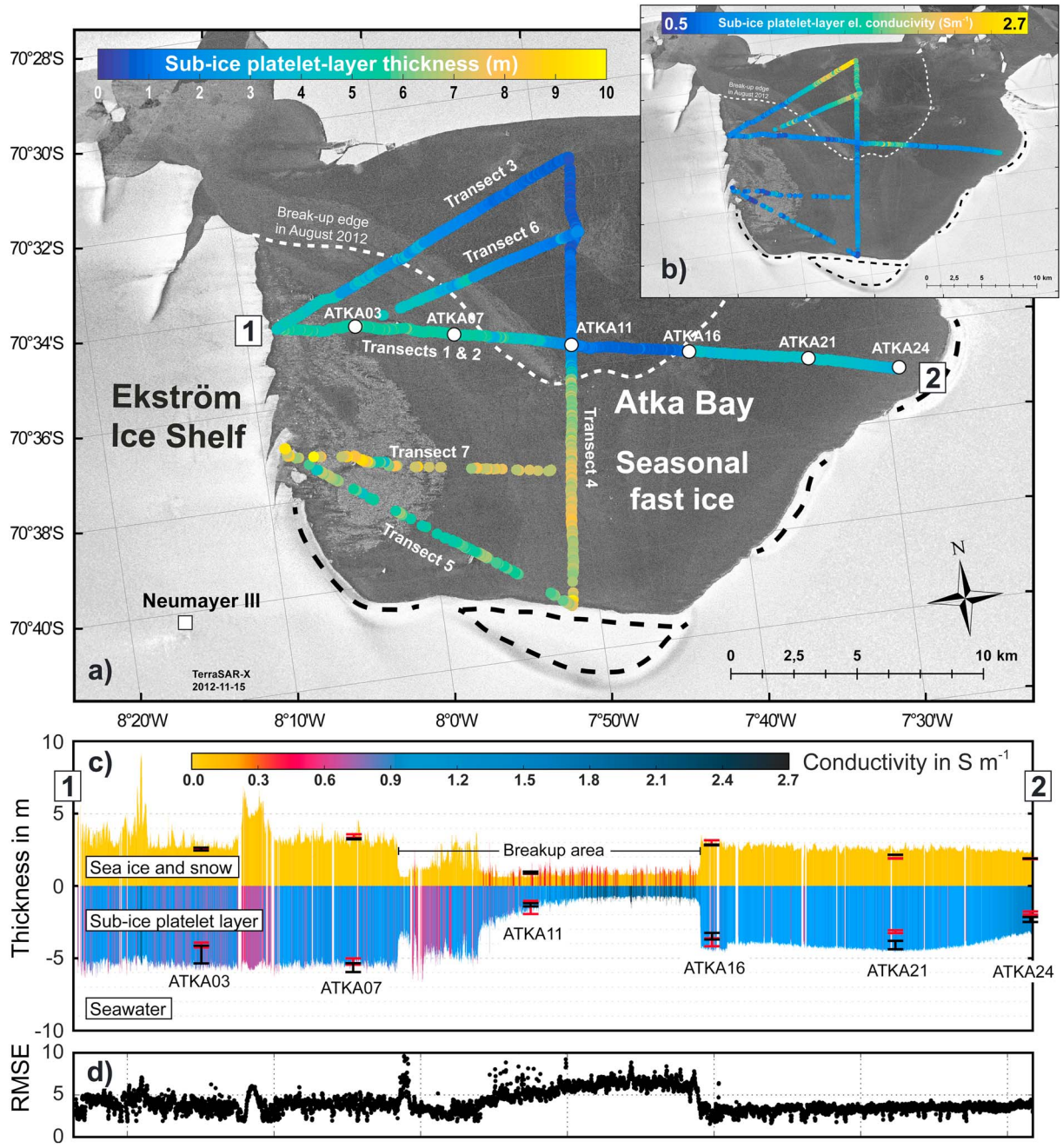

Figure 1. (a) Platelet layer thickness and (b) electrical conductivity below Atka Bay landfast sea ice, obtained from a laterally constrained Marquardt-Levenberg inversion of multifrequency EM data. Background: TerraSAR-X image from 15 November 2012, provided by the German Aerospace Agency (DLR). The ice sheet is grounded at several locations, forming ice rises and rumples (dashed black lines). The August 2012 sea ice breakup edge (dashed white line) and sites of regular drillings (white circles with black outline) are also indicated. (c) Sea ice and platelet layer thickness and conductivity from inversion of Transect 2 (between "1" and "2" indicated in Figure 1a), along with the range of simultaneous drill hole measurements obtained in November (red bars) and December 2012 (black bars). (d) Corresponding root-mean-square errors (RMSE) of field data inversions.

interfaces in the vertical and smooth horizontal conductivity gradients within each layer. Because of the pronounced increase in conductivity with depth, the three-layer case of sea ice, platelet layer, and seawater is an ideal target for the inversion of electromagnetic induction sounding data [*Spies and Frischknecht*, 1991]. Although the snow cover usually exhibits a much lower electrical conductivity than sea ice (or much higher in case of surface flooding), we regard sea ice and snow as one layer. This simplification was a necessary compromise to not further complicate the retrieval of the platelet layer parameters, which was our main aim.

To account for the sharp conductivity interfaces between the layers, we used a 1-D Marquardt-Levenberg (ML) inversion [*Lines and Treitel*, 1984] implemented in the software package EMILIA: Electromagnetic Inversion with Least Intricate Algorithms [*Grab*, 2012; *Kalscheuer*, 2014; *Kaufmann*, 2014; *Kalscheuer et al.*, 2015]. In contrast to an inversion in which the only free parameters are the conductivities in multiple fixed layers [e.g., EM1DFM, *Farquharson et al.*, 2003], the ML inversion can directly invert for thicknesses without the need for evaluating a broad conductivity transition zone. In order to test the general performance and reliability of the ML inversion, we first created and inverted a synthetic data set with different starting models (Text S2 and Figure S3 in the supporting information), following the method of *Hunkeler et al.* [2016]. To determine which model parameters are constrained well by our data, we performed a nonlinear most-squares inversion [*Meju and Hutton*, 1992; *Kalscheuer and Pedersen*, 2007; *Kalscheuer et al.*, 2015, Text S2 and Table S4 in the supporting information]. Finally, we used a laterally constrained ML inversion [*Auken et al.*, 2005; *Kaufmann*, 2014] for field data processing, resulting in a pseudo 2-D model.

All inversions were performed using the above-mentioned three layers, allowing for four free parameters: (1) sea ice plus snow thickness and (2) conductivity, as well as (3) platelet layer thickness and (4) conductivity. The seawater layer was considered as a homogeneous half-space with a constant conductivity of 2.7 S m^{-1}.

For each inversion model, we calculated the root-mean-square error (RMSE):

$$\mathrm{RMSE} = \sqrt{\frac{1}{N}\sum_{i=1}^{N}\left(\frac{d_{\mathrm{meas},i} - d_{\mathrm{cal},i}}{\sigma_{d,i}}\right)^2}, \tag{1}$$

where N is the number of measurements, i is a data index, $d_{\mathrm{meas},i}$ is the ith measured signal, $d_{\mathrm{cal},i}$ is the ith calculated signal of the subsurface model, and $\sigma_{d,i}$ is the estimated uncertainty of $d_{\mathrm{meas},i}$. An inversion model with a RMSE close to 1 is considered optimal, because the model response explains the measured data without fitting too much to the noise which is contained in the data [*Kalscheuer et al.*, 2013].

2.2.1. Transects and Laterally Constrained ML Inversion

The transect data were filtered to obtain a spacing of 4 m between measurements, in order to reduce the computing time. All data were corrected using instrument-specific calibration coefficients, and the uncertainties for in-phase and quadrature recordings at all frequencies were determined from noise measurements in free air [*Hunkeler et al.*, 2015].

In *Hunkeler et al.* [2016], individual 1-D models were stitched together to get a 2-D impression of the inversion results along a transect. To build a laterally smooth 2-D model, the ML inversion was augmented with horizontal smoothness constraints that were implemented as first-order differences of the layer parameters between adjacent stations [*Kaufmann*, 2014]. The resulting pseudo 2-D model contains distinct layers but smooth lateral variations of conductivity and thickness within each layer. Since we expect the layer thicknesses of adjacent stations to vary more than their conductivities, we weighted the penalty on conductivity variation four times that of thickness variation. We allowed for a maximum of 100 iterations.

In all inversions of field data, we used a starting model of 1 m with a conductivity of 0.05 S m^{-1} (representing sea ice plus snow), 2 m with 1.15 S m^{-1} (representing the platelet layer), and a homogeneous half-space with 2.7 S m^{-1} (representing seawater).

After the inversion, we excluded stations with a RMSE > 10 from all further calculations. This threshold was determined by visual inspection of the results, omitting outliers and implausible values. We additionally defined upper and lower conductivity thresholds for the platelet layer at 2.7 and 0.5 S m^{-1}, between which the model was considered plausible.

3. Results

3.1. Sea Ice and Platelet Layer Spatial Variability

Figures 1a and 1b show the filtered platelet layer thicknesses (t_p) and conductivities (σ_p), calculated from the inversion of the multifrequency EM field data. The background shows a TerraSAR-X image from 15 November 2012, obtained shortly before the GEM-2 transects. t_p ranged between 0.3 and 9.15 m, with the lowest values (<2 m) within the August breakup area and the highest (7–9.15 m) in the southern half. t_p generally increased toward the ice shelf edges bordering the bay in the west and south but decreased toward the eastern margin. σ_p covered the entire allowed range from 0.5 to 2.7 S m^{-1}, with the highest values in the August breakup area.

Figure 1c gives a more detailed view of the inversion results of Transect 2, which followed a regular route between the northern sea ice ramp (labeled "1") and the westernmost point, ATKA24 (labeled "2"). In total, 291 of 6442 stations from Transect 2 exceeded the quality threshold of RMSE >10 (Figure 1d) or exhibited a platelet layer conductivity <1 and >2.7 S m^{-1}. These stations are not shown here.

The combined sea ice plus snow thickness t_s in Transect 2 (plotted on the positive *y* axis) ranged between 0.56 and 9.15 m. A thin sea ice plus snow layer was found in the breakup area, whereas the largest t_s was found in the dynamically deformed area in the west. Thick sea ice plus snow between ATKA03 and ATKA07 is the result of snow accumulation behind an iceberg. t_s in the eastern part of the bay was mainly thermodynamically grown and was therefore generally more homogeneous compared to the deformed ice regime in the west (also indicated by a region of higher backscatter in the TerraSAR-X image). The present results are generally consistent with an earlier study [*Hoppmann et al.*, 2015b], in which the overall snow and sea ice conditions at Atka Bay in 2012 were discussed in more detail. The combined conductivity of sea ice plus snow, σ_s, varied between 0.013 and 0.538 S m^{-1}. Highest conductivities were found in the breakup area, most likely corresponding to extended surface flooding which were also observed in the field.

The platelet layer thickness t_p (plotted on the negative *y* axis) ranged between 0.63 and 6.63 m. In the western part of the bay, t_p was generally homogeneous and on average about 1 m thicker than in the eastern part. In the breakup area, t_p was characterized by a high variability at the western breakup edge, a continuous decrease near ATKA11, and a sharp transition at the eastern breakup edge near ATKA16. The platelet layer conductivity σ_p covered the entire allowed range. The highest σ_p was found in the breakup area, whereas the lowest values were observed in strongly deformed areas and at the locations of the thickest sea ice plus snow. The latter data have to be interpreted with care, since they are likely an indication of the limits of the method.

The EM-derived thickness results for both, sea ice and platelet layer thickness, are within the uncertainty range of drillhole measurements obtained at regular sampling sites on 17 November 2012 (red bars in Figure 1c) and 14 December 2012 (black bars). The bars show the total range of up to five measurements taken at each site. The level of agreement between t_p and the manual measurements is remarkable, especially when taking into account that the manual measurements by the metal bar method likely underestimated the true thickness by up to 0.3 m [*Hoppmann et al.*, 2015b].

3.2. Thickness and Conductivity Distributions

The probability density distribution (pdd) of t_s (Figure 2b) show peaks at 0.8 and 2.6 m, representing (1) the thermodynamically grown fast ice formed in the breakup area in October and (2) the older fast ice formed in May. The pdd of t_p (Figure 2a) reveals a distribution with four peaks at 0.8, 4.3, 5.4, and 6.6 m. These represent the conditions (1) in the breakup area, (2) in the eastern part of the bay, (3) in the western part, and (4) in the south. The corresponding 2-D histogram (Figure 2d) underlines the correlation between the two pdds, where a larger platelet layer thickness corresponds to a larger sea ice thickness.

The pdd of σ_p shows a broad distribution, with a peak at around 0.9 S m^{-1} (Figure 2c). The 2-D histogram of σ_p and t_p reveals an inversely proportional dependency (Figure 2e), where a thicker platelet layer is accompanied by a low conductivity.

3.3. Platelet Layer Ice Volume Fraction

As demonstrated in *Hunkeler et al.* [2015], we converted σ_p to an ice volume fraction β using Archie's law [*Archie*, 1942]:

$$\beta = 1 - \sqrt[m]{\frac{\sigma_p}{\sigma_b}}, \tag{2}$$

where σ_b is the brine conductivity, which is assumed to correspond to the seawater conductivity (2.7 S m^{-1}), m is the cementation factor, and β is 1 minus the porosity Φ. The cementation factor is an empirical factor, which depends on the pore geometry, its connectivity, and the shape of the ice platelets. However, their influence on m is not well known for the platelet layer [*Hunkeler et al.*, 2015].

The distribution of β is shown in Figure 2f for $m = 3$. The mean, median, and standard deviation are 0.26, 0.28, and 0.09, respectively. Depending on the choice of m, the distribution of β shifts to smaller ($m > 3$) or higher ($m < 3$) values (Figure 2g, with mean ice volume fractions on vertical axis). For $m = 2$, for example, the mean, median, and standard deviation are 0.36, 0.39, and 0.12, respectively. For $m = 4$, the mean, median, and standard deviation are 0.2, 0.22, and 0.07, respectively.

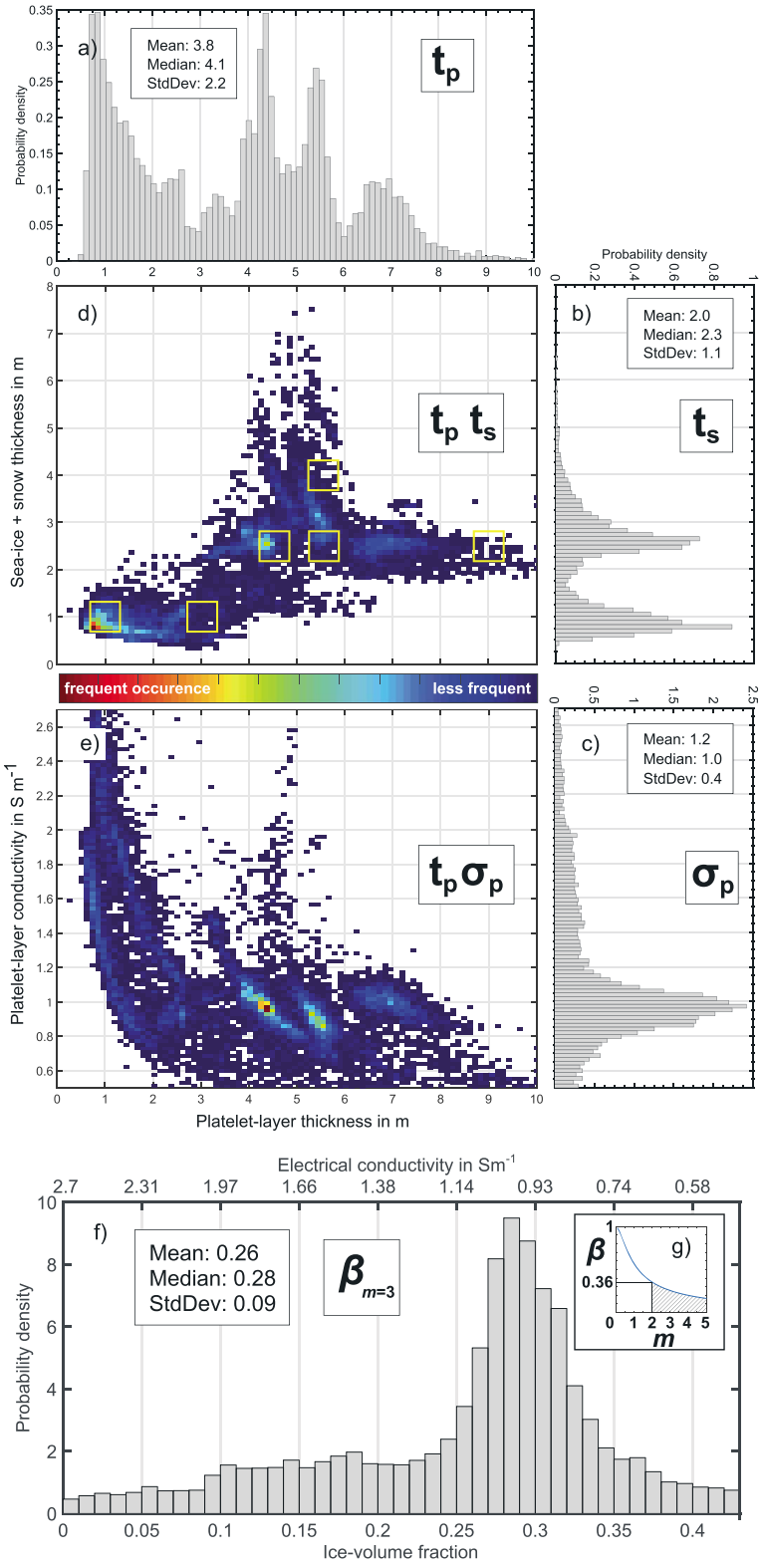

Figure 2. Probability density distribution of Transects 2–7 of (a) platelet layer thickness t_p, (b) sea ice plus snow thickness t_s, and (c) platelet layer conductivity σ_p. Two-dimensional histograms of (d) platelet layer versus sea ice plus snow thickness and (e) platelet layer thickness versus platelet layer conductivity. Yellow squares in Figure 2d indicate the thicknesses used for most-squares inversions of synthetic data (Table S4). (f) Distribution of platelet layer ice volume fractions (β) calculated from Archie's law, assuming a cementation factor $m = 3$. (g) Relationship between m and β [*Archie*, 1942] for our conductivity data set. Plausible values for β are achieved for $m > 2$ (dashed area).

4. Discussion

4.1. Reliability and Limits of the Presented Method

The great complexity of multifrequency EM sensor calibration and data inversion presents many potential error sources, and care has to be taken when interpreting the results. In the present study we tried to ensure the reliability of the method by (1) performing sensitivity studies and most-squares inversions, (2) checking the consistency by comparison to earlier studies, and (3) validating the final results using drill hole measurements. Combining all the results, we were able to demonstrate the potential to simultaneously determine sea ice and sub-ice platelet layer thickness and conductivity using a carefully calibrated, multifrequency EM instrument in combination with a suitable inversion algorithm. However, in order to achieve reliable results, an absolute calibration of the instrument (as described in detail in *Hunkeler et al.* [2015]) and a carefully prepared inversion algorithm (accounting for passive bucking as described in *Hunkeler et al.* [2016]) are crucial prerequisites.

The proposed method also has its limits and caveats, some of which warrant further discussions. First, the lowest RMSE for each transect was found after iteration 100, the defined maximum value. Higher RMSE values in field data inversion compared to synthetic data inversion may originate from 2-D or 3-D structure of the sea ice and platelet layer and the higher number of stations. Systematic errors, like an incorrect calibration or the drift of the instrument, as well as tilt of the EM instrument in the kayak, provide an additional error source, high RMSE, thus slow convergence. Furthermore, for the inversion to converge at adequate speed, the applied ML damping requires the start model to be relatively close to the true model. Hence, with an increasing number of stations, a start model which is the same for all stations (as used in this study) may pose increasing difficulty to obtain convergence. The highest RMSE values of individual stations were found (and excluded from further processing for RMSE >10) for the transects in which the sea ice plus snow layer was especially thick (Transect 5 and 7, Figure 1a).

Second, the calculations were performed under the assumption of three distinct, locally homogeneous layers. However, field measurements of sea ice or platelet layer thickness often revealed inhomogeneities in either layers, especially in the more deformed sea ice. Inverting for only three layers is therefore an oversimplification but is needed to study the main parameter of interest, the platelet layer thickness. The results of the synthetic study indicated that a retrieval of platelet layer thickness is poorly constrained for relatively thick sea ice and platelet layers (Figures S3b and S3h and Table S4). However, most of the field data were in a range which yielded reliable results (1 m $< t_p <$ 7 m), a finding which was confirmed by the generally plausible geographical distribution pattern (Figure 1a) and the good agreement with simultaneous drill hole measurements (Figure 1c).

Third, interior melt of fast ice in summer [*Hoppmann et al.*, 2015a] leads to an increased permeability. Once a certain permeability threshold is reached, it may lead to surface flooding, given that the snow load on top is high enough to suppress the sea ice surface below the water level. By this process, a highly conductive layer of slush is formed on top of the sea ice. This process was directly observed in the breakup area around ATKA11 but also evident in the inversion results (Figure 1c, red tones within yellow area). Since it is in principle possible to determine the presence of surface flooding from EM data [*Hunkeler et al.*, 2015], we performed additional experiments trying to invert for a conductive layer on top of the sea ice. However, our results (not shown here) were not able to accurately resolve this additional layer. It is likely that the sea ice layer itself was highly porous, resulting in high conductivities.

4.2. Geophysical Implications of the Data

Under the assumption that the results produced by our method are reliable, the EM-derived data enhance the understanding of the complex processes and interactions between ocean, ice shelf, and sea ice in several ways. Discussion of the data set in exhaustive detail is beyond the scope of this paper, but in the following we highlight three important aspects.

First, it is now possible to more accurately determine the contribution of ocean/ice shelf interaction to sea ice mass balance in the study area and to relate the overall volume to ice shelf basal melt volume of the Ekström Ice Shelf. In their study, *Hoppmann et al.* [2015b] assumed an average platelet layer thickness of 4 m based on the drill hole measurements indicated in Figure 1 to show that ice platelets contribute 43% to total sea ice mass at Atka Bay, corresponding to 22% of the Ekström Ice Shelf annual basal melt volume. The sub-ice platelet layer thickness distribution from our study reveals that the point measurements from Transect 2 do not account for the thicker platelet layer in the southern half of the bay, leading to an overall underestimation of the average

platelet layer thickness of up to 1.3 m (neglecting the area of young ice in the breakup area). Using the corrected average thickness of 5.3 m, the contribution of ocean/ice shelf interaction to annual (first-year) sea ice mass in this region is 49%, representing about 27% of the annual annual ice-shelf basal melt volume. Since Transect 2 is also the basis of ongoing sea ice monitoring activities, it needs to be considered to relocate or add measurement sites in the southern Atka Bay (i.e., including Transect 4) to more accurately determine the average annual ice platelet accumulation.

Second, the thickness and conductivity maps in Figure 1 are useful to identify outflow regions of ice crystals in a supercooled plume [*Robinson et al.*, 2014; *Hughes et al.*, 2014]. The observed north-south and east-west gradients of platelet layer thickness (with thicker platelet layers in the south and in the west) indicate either an enhanced accumulation in that region or a redistribution toward the southwest. There are, however, several indications that the main outflow area is in the central western part of Atka Bay and that currents redistribute suspended and loosely attached ice platelets toward the eastern part of the bay:

1. The thickness pattern from Transect 2 (Figure 1c), especially the generally decreasing thickness toward the east and the gradual decrease near ATKA11, suggests that platelets are advected toward the east. Eastward currents are, in general, not expected close to the Antarctic continent since the Antarctic Coastal Current flows mainly westwards. However, *Fahrbach et al.* [1992] reported a weak current in our study area which is influenced by sea floor topography and tides. Also, *Hoppmann et al.* [2015b] concluded that the platelet release might be related to episodic events connected to tides.
2. The rather small part of the Ekström Ice Shelf, which lies east of Atka Bay, is likely not a source of supercooled water due to the limited depth. The more likely source is the deep part of the western Ekström Ice Shelf several hundred kilometers to the south.
3. Due to the presence of several ice rises and ice rumples (where the ice sheet is grounded) in the southwest, south, and east of the bay (dashed black lines in Figure 1), there are only a few locations where the plume could emerge from below the ice shelf.
4. Episodic events of platelet-layer riseup from below were recorded by cameras in the western part of the bay [*Hoppmann et al.*, 2015b].

In order to draw more conclusions about the main ice shelf outflow areas, the entire ice shelf edge, and especially the passages between the areas of grounded ice, need to be covered by EM transects.

Third, the conductivity retrieved from the inversion (Figure 1b) gives an impression of the relative compaction of the ice platelets. Higher conductivities found in the sea ice breakup area, where a relatively new platelet layer formed from October on, are related to a higher seawater content in the pore space between the platelets. Lower platelet layer conductivities below the more typical first-year sea ice in other parts of the bay are an indication of more ice and less seawater in the interstices. These findings are generally consistent with drill hole measurements, where the mechanical resistance during platelet layer thickness measurements was significantly lower in the area of newer platelet layers. In general, conductivity is higher for a thinner and younger platelet layer, which implies that an older thick platelet layer is more compacted and denser than a young thin platelet layer (Figure 2e). A thicker platelet layer is potentially more compressed because of increased buoyancy of underlying platelets and compaction due to ocean currents, leading to lower conductivity.

The conversion of electrical conductivity to ice volume fraction was performed using Archie's law (equation (2)), a procedure which very much depends on a yet not well known cementation factor. *Hunkeler et al.* [2015] used calibration measurements over thin sea ice and platelet layer at site ATKA11 to calculate a mean platelet layer conductivity of 1154 ± 271 S m^{-1}. The conversion to ice volume fraction yielded values of 0.29 ($m = 2.5$) to 0.43 ($m = 1.5$). These results were too high compared to other recent studies, which found ice volume fractions of 0.25 ± 0.06 [*Gough et al.*, 2012], 0.16 ± 0.07 [*Price et al.*, 2014], 0.22 [*Wongpan et al.*, 2015], and 0.18 ± 0.09 [*Hoppmann et al.*, 2015a]. In Figure 2g, the relation between the average ice volume fraction and cementation factor m is shown using our electrical conductivity data set. By using a higher m, the ice volume fraction is shifted toward higher values. To obtain the best agreement with the ice volume fractions suggested by the studies mentioned above, a cementation factor of $m = 3$ or even higher may need to be considered. Only a limited number of studies are available which empirically determined a cementation factor for disc-shaped geometries: *Jackson et al.* [1978], for example, used platy shell fragments with a sphericity of 0.5 and found a cementation factor of 1.9. But loose platelets may even be less spherical, which would lead to a higher cementation factor. However, for further studies it might be necessary to model cementation factors for different platelet layer arrangements.

5. Conclusions

In this study, we obtained a substantial multifrequency EM induction sounding data set on an Antarctic fast ice regime with an underlying platelet layer. We calculated fast ice and platelet layer thicknesses and conductivities, using this unique data set as an input for a laterally constrained Marquardt-Levenberg inversion scheme. Our results provide evidence that platelet layer thickness retrieval is possible from the surface using a nondestructive method, a finding which we expect to significantly facilitate its volume estimation in the future. Given that the sub-ice platelet layer is one of the most productive marine habitats, biological studies would also benefit from such kind of data. The high-resolution achieved with this method is suitable to reveal accumulation patterns and identify ice shelf outflow regions, albeit complementary oceanographic measurements are still needed. The presented methodology is a crucial step in determining the relative contribution of subice shelf processes to sea ice mass balance in the Southern Ocean and hence a valuable tool to better understand ocean/ice shelf interaction without the need for extensive logistics. However, this study is only a starting point, and it is necessary to repeat measurements for time series and to collect more multifrequency data on other sea ice sites in coastal Antarctica. The current limitation to spatial scales of up to 100 km due to operation by snowmobiles could be overcome by an adaptation of this methodology to airborne multifrequency EM measurements.

Acknowledgments

This work would not have been possible without the Neumayer III infrastructure and the help of the wintering crew 2012. The authors are grateful to Stephan Paul and Uwe Baltes for their assistance in the field and to the AWI logistics for their support. The computations were performed on resources provided by SNIC through Uppsala Multidisciplinary Center for Advanced Computational Science (UPPMAX) under project snic2014-1-243. Johan Hermansson at UPPMAX is acknowledged for his assistance concerning technical and implementational aspects in making the code run on the UPPMAX resources. This work was funded by the POLMAR graduate school and the German Research Council (DFG) in the framework of its priority program "Antarctic Research with comparative investigations in Arctic ice areas" by grants to SPP1158, NI 1092/2, and HE2740/12. The data used here are publicly available at http://doi.pangaea.de/10.1594/PANGAEA.845535. Finally, we thank the anonymous reviewers whose comments and suggestions significantly improved the manuscript.

References

Archie, G. E. (1942), The electrical resistivity log as an aid in determining some reservoir characteristics, *Transactions of the AIME*, *146*, 54–62, doi:10.2118/942054-G.

Auken, E., A. V. Christiansen, B. H. Jacobsen, N. Foged, and K. I. Sørensen (2005), Piecewise 1D laterally constrained inversion of resistivity data, *Geophys. Prospect.*, *53*(4), 497–506, doi:10.1111/j.1365-2478.2005.00486.x.

Bintanja, R., G. J. van Oldenborgh, S. S. Drijfhout, B. Wouters, and C. A. Katsman (2013), Important role for ocean warming and increased ice-shelf melt in Antarctic sea-ice expansion, *Nat. Geosci.*, *6*(5), 376–379, doi:10.1038/ngeo1767.

Crocker, G. (1988), Physical processes in Antarctic landfast sea ice, PhD thesis, Univ. of Cambridge, Cambridge, U. K.

Eicken, H., and M. A. Lange (1989), Development and properties of sea ice in the coastal regime of the southeastern Weddell Sea, *J. Geophys. Res.*, *94*(C6), 8193–8206, doi:10.1029/JC094iC06p08193.

Fahrbach, E., G. Rohardt, and G. Krause (1992), The antarctic coastal current in the southeastern Weddell Sea, *Polar Biol.*, *12*(2), 171–182, doi:10.1007/BF00238257.

Farquharson, C. G., D. W. Oldenburg, and P. S. Routh (2003), Simultaneous 1D inversion of loop-loop electromagnetic data for magnetic susceptibility and electrical conductivity, *Geophysics*, *68*(6), 1857–1869, doi:10.1190/1.1635038.

Gough, A. J., A. R. Mahoney, P. J. Langhorne, M. J. M. Williams, N. J. Robinson, and T. G. Haskell (2012), Signatures of supercooling: McMurdo Sound platelet ice, *J. Glaciol.*, *58*(207), 38–50, doi:10.3189/2012JoG10J218.

Grab, M. (2012), Forward and inverse modelling of frequency-domain electromagnetic data from small coils, Master thesis, IDEA League, ETH Zurich, Switzerland.

Günther, S., and G. S. Dieckmann (1999), Seasonal development of algal biomass in snow-covered fast ice and the underlying platelet layer in the Weddell Sea, Antarctica, *Antarct. Sci.*, *11*(3), 305–315, doi:10.1017/S0954102099000395.

Hellmer, H. H. (2004), Impact of Antarctic ice shelf basal melting on sea ice and deep ocean properties, *Geophys. Res. Lett.*, *31*, L10307, doi:10.1029/2004GL019506.

Hoppmann, M., M. Nicolaus, S. Paul, P. A. Hunkeler, P. Heil, L.-K. Behrens, G. König-Langlo, and R. Gerdes (2015a), Seasonal evolution of an ice-shelf influenced fast-ice regime, derived from an autonomous thermistor chain, *J. Geophys. Res. Oceans*, *120*, 1703–1724, doi:10.1002/2014JC010327.

Hoppmann, M., et al. (2015b), Ice platelets below Weddell Sea land-fast sea ice, *Ann. Glaciol.*, *56*(69), 175–190, doi:10.3189/2015AoG69A678.

Hughes, K. G., P. J. Langhorne, G. H. Leonard, and C. L. Stevens (2014), Extension of an Ice Shelf Water plume model beneath sea ice with application in McMurdo Sound, Antarctica, *J. Geophys. Res. Oceans*, *119*, 8662–8687, doi:10.1002/2013JC009411.

Hunkeler, P. A., S. Hendricks, M. Hoppmann, S. Paul, and R. Gerdes (2015), Towards an estimation of sub-sea-ice platelet-layer volume with multi-frequency electromagnetic induction sounding, *Ann. Glaciol.*, *56*(69), 137–146, doi:10.3189/2015AoG69A705.

Hunkeler, P. A., S. Hendricks, M. Hoppmann, C. G. Farquharson, T. Kalscheuer, M. Grab, M. S. Kaufmann, L. Rabenstein, and R. Gerdes (2016), Improved 1D inversions for sea ice thickness and conductivity from electromagnetic induction data: Inclusion of nonlinearities caused by passive bucking, *Geophysics*, *81*(1), WA45–WA58, doi:10.1190/geo2015-0130.1.

Jackson, P., D. T. Smith, and P. Stanford (1978), Resistivity-porosity-particle shape relationships for marine sands, *Geophysics*, *43*(6), 1250–1268, doi:10.1190/1.1440891.

Jordan, J. R., S. Kimura, P. R. Holland, A. Jenkins, and M. D. Piggott (2015), On the conditional frazil ice instability in seawater, *J. Phys. Oceanogr.*, *45*(4), 1121–1138, doi:10.1175/JPO-D-14-0159.1.

Kalscheuer, T. (2014), EMILIA—Electromagnetic inversion with least intricate algorithms user manual, *Tech. Rep.*, Uppsala Univ., Dep. of Earth Sci., Uppsala, Sweden.

Kalscheuer, T., and L. B. Pedersen (2007), A non-linear truncated SVD variance and resolution analysis of two-dimensional magnetotelluric models, *Geophys. J. Int.*, *169*(2), 435–447, doi:10.1111/j.1365-246X.2006.03320.x.

Kalscheuer, T., M. Bastani, S. Donohue, L. Persson, A. Pfaffhuber, F. Reiser, and Z. Ren (2013), Delineation of a quick clay zone at Smørgrav, Norway, with electromagnetic methods under geotechnical constraints, *J. Appl. Geophys.*, *92*, 121–136.

Kalscheuer, T., et al. (2015), Joint inversions of three types of electromagnetic data explicitly constrained by seismic observations: Results from the central Okavango Delta, Botswana, *Geophys. J. Int.*, *202*(3), 1429–1452.

Kaufmann, M. S. (2014), Pseudo 2D inversion of multi-frequency coil-coil FDEM data, Master thesis, IDEA League, ETH Zurich, Switzerland.

Kipfstuhl, J. (1991), On the formation of underwater ice and the growth and energy budget of the sea ice in Atka Bay, Antarctica (Zur Entstehung von Unterwassereis und das Wachstum und die Energiebilanz des Meereises in der Atka Bucht, Antarktis, mostly in German), Reports on Polar and Marine Research, *Ber. Polarforsch.*, *85*, 1–88.

Langhorne, P. J., et al. (2015), Observed platelet ice distributions in antarctic sea ice: An index for ocean-ice shelf heat flux, *Geophys. Res. Lett.*, *42*, 5442–5451, doi:10.1002/2015GL064508.

Lewis, E. L., and R. G. Perkin (1986), Ice pumps and their rates, *J. Geophys. Res.*, *91*(C10), 11,756–11,762, doi:10.1029/JC091iC10p11756.

Lines, L. R., and S. Treitel (1984), Tutorial: A review of least-squares inversion and its application to geophysical problems, *Geophys. Prospect.*, *32*(2), 159–186.

Meju, M., and V. Hutton (1992), Iterative most-squares inversion: Application to magnetotelluric data, *Geophys. J. Int.*, *108*(3), 758–766, doi:10.1111/j.1365-246X.1992.tb03467.x.

Price, D., W. Rack, P. J. Langhorne, C. Haas, G. Leonard, and K. Barnsdale (2014), The sub-ice platelet layer and its influence on freeboard to thickness conversion of Antarctic sea ice, *Cryosphere*, *8*(3), 1031–1039, doi:10.5194/tc-8-1031-2014.

Rack, W., C. Haas, and P. J. Langhorne (2013), Airborne thickness and freeboard measurements over the McMurdo Ice Shelf, Antarctica, and implications for ice density, *J. Geophys. Res. Oceans*, *118*, 5899–5907, doi:10.1002/2013JC009084.

Robinson, N. J., M. J. M. Williams, C. L. Stevens, P. J. Langhorne, and T. G. Haskell (2014), Evolution of a supercooled Ice Shelf Water plume with an actively growing subice platelet matrix, *J. Geophys. Res. Oceans*, *119*, 3425–3446, doi:10.1002/2013JC009399.

Spies, B. R., and F. C. Frischknecht (1991), Electromagnetic sounding, in *Electromagnetic Methods in Applied Geophysics*, vol. 2, Applications, Parts A, pp. 285–426, Soc. of Exploration Geophys., Okla.

Vacchi, M., M. Mesa, and S. Greco (2000), The coastal fish fauna of Terra Nova Bay, Ross Sea, Antarctica, in *Ross Sea Ecology*, vol. 32, edited by F. M. Faranda, L. Guglielmo, and A. Ianora, pp. 457–468, Springer, Berlin, doi:10.1007/978-3-642-59607-0_32.

Wongpan, P., P. J. Langhorne, D. E. Dempsey, L. Hahn-Woernle, and Z. Sun (2015), Simulation of the crystal growth of platelet sea ice with diffusive heat and mass transfer, *Ann. Glaciol.*, *56*(69), 127–136, doi:10.3189/2015AoG69A77.